Annealing time-dependent evolution of morphology and luminescence behavior of zinc oxide thin films

ZHEN TIAN[1], LINHUA XU[1,2,*], AOXIN ZANG[1], WENYANG MA[1]
[1]*School of Physics and Optoelectronic Engineering, Nanjing University of Information Science and Technology, Nanjing 210044, China*
[2]*Laboratory for Optoelectronic Functional Materials and Devices, Nanjing University of Information Science and Technology, Nanjing 210044, China*

The tailoring of optical properties of ZnO films caused by the evolution of the morphology is a subject of great concern. In this research, Al, Fe and Cl (Al-Fe-Cl) incorporated ZnO films were deposited by the sol-gel technique and the annealing time-dependent evolution of morphology and optical properties were analyzed in detail. The results show that pyramid-like grains are formed on the film surface after annealing treatment. When the annealing time exceeds 1 h, the pyramid-like grains on the film surface begin to aggregate. With the further increase of the annealing time, the aggregation of the pyramid-like grains becomes more obvious. In addition, the increase of annealing time greatly changes the luminescence behavior of ZnO thin films.

(Received December 26, 2022; accepted June 6, 2023)

Keywords: ZnO films, Sol-gel method, UV emission, Annealing time, Surface aggregation of grains

1. Introduction

Zinc Oxide (ZnO) is a very important wide bandgap semiconductor. Nanoscaled ZnO material exhibits novel optical, magnetic and electrical properties [1-5], which make it be applicable to many devices and new technology fields such as linear-piezoelectric actuators [6], ultraviolet photodetectors [7, 8], thin film transistors [9], anti-reflection layers in solar cells [10], triethanolamine sensors [11], photocatalysts [12, 13], light-emitting devices [14, 15], etc. At present, there are many methods for preparing nano-ZnO thin films, among which the sol-gel process is recommended by many researchers due to some outstanding advantages. These outstanding advantages include molecular-level doping, low cost, high purity of the films, simple operation, and easy preparation of multi-component metal oxide films [16]. Previously, Phan et al. [17] found that compared with ZnO thin films prepared by magnetron sputtering, those prepared by sol-gel method were more suitable for optoelectronic or UV/blue light devices at the nanoscale. It is well known that the metal-oxide thin films fabricated by the sol-gel process need proper heat-treatment to remove the solvent and other organic substances in the sol films and make the films crystallize. Therefore, the physical characteristics of ZnO films prepared by sol-gel technique are more dependent on heat-treatment conditions than those deposited by other techniques. Sengupta et al. [18] reported that different annealing temperatures greatly changed the growth orientation, morphology, transmittance and bandgap of ZnO films fabricated by sol-gel technique. Yatskiv et al. [19] found that the emitted photon energy from ZnO film prepared with a sol-gel technique could be gradually converted from 2.8 eV (blue light) to 1.8 eV (red light) by thermally treating it in air and argon at different temperatures. Kim et al. [20] grew ZnO thin films using the sol-gel technique on glass substrates, and found that different annealing ways significantly changed the surface morphology of the films.

In a previous study, we reported the influence of Al-Fe-Cl incorporation on the morphology, microstructure and photoluminescence behavior of ZnO films [21]. It was found that the co-doping of Al and Cl resulted in the occurrence of many pyramidal grains with high-quality on the surface of ZnO thin films, which led the films to have a strong UV emission. The presence of Fe did not influence the formation of the pyramidal grains with high crystal quality and seemed to be more favorable for the improving the density of the films. In view of the attractive optical properties exhibited by the films and the wide potential utilizations of Al-Fe-Cl co-doped ZnO films [22, 23], in this research, we further explored the impact of annealing time on ZnO thin films co-doped with Al, Fe and Cl ions fabricated by sol-gel process. The results show that with the prolongation of annealing time, the pyramid-shaped grains on the film surface gradually aggregate and significantly affect the photoluminescence behavior, while the polycrystalline ZnO layer at the bottom of the film slightly changes. To our knowledge, ZnO coatings deposited by sol-gel method exhibiting different structural evolution with heat treatment time have rarely been reported.

2. Experimental

The films were fabricated by spin-coating sol technique. Firstly, a precursor solution for ZnO was

prepared by the following steps. $Zn(CH_3COO)_2•2H_2O$, $Fe(NO_3)_3•9H_2O$ and $AlCl_3•6H_2O$ were put into ethanol according to a certain percentage. The mixture was stirred for 1 h at 65 ^oC. At the same time, monoethanolamine as a stabilizer was added into the mixture drop by drop. Then, homogeneous and clear ZnO sol was obtained. The concentration of zinc acetate was 0.4 mol/L. The doping concentrations of Al and Fe were 12 and 3 at.%, respectively, relative to Zn. After the sol was hermetically placed for 24 h, it was spin-coated on a substrate which was not heated to form a sol layer. The substrate with the sol-layer was placed in air for 2 min and then preheated at 300 ^oC for 4 min in a muffle furnace. The process from coating sol-layer to preheat-treatment was performed 8 times. Finally, the ZnO coatings were annealed at 450 ^oC. To investigate the effect of different annealing times on Al-Fe-Cl co-doped ZnO films, six samples were annealed for 0, 0.5, 1.0, 1.5, 2.0 and 2.5 h, respectively. The annealing process was performed in an air atmosphere.

The surface morphology of the films was examined by field emission scanning electron microscopy (FE-SEM, S-4800). The crystallographic structures of the films were analyzed by X-ray diffractometer (XRD, Bruker D8). The composition and the distribution of doped elements were determined by an energy dispersive spectrometer (EDS) attached to the FE-SEM. The surface composition and valence state of the elements were investigated by an X-ray photoelectron spectrometer (XPS, Thermo escalab 250Xi). The photoluminescence (PL) behavior of the samples was studied using a spectrometer with an excitation wavelength of 325 nm.

3. Results and discussion

Crystal structure features of the films subjected to different annealing times are revealed by XRD patterns which are illustrated in Fig. 1. The unannealed sample exhibits a very weak (002) diffraction peak, indicating that the ZnO grains in this sample are small and it contains a large amount of amorphous components. After annealing all samples exhibit two diffraction peaks, namely (002) and (004) peaks. This confirms that the films are highly oriented toward the c-axis direction. When the annealing time exceeds 60 min, the intensity of the (002) peak gradually decreases. This indicates that the growing trend of ZnO grains toward the c-axis is weakened. From the FE-SEM images in Fig. 2, it can be known that when the annealing time exceeds 60 min, the pyramid-shaped nanostructures on the film surface begin to aggregate. The growth mode of the grains on the film surface changed from vertical growth to lateral growth, which led to the decline of the (002) peak intensity. Although the doping concentration of Al is high, there is no impurity phase associated with it, such as zinc aluminate, alumina, etc. Previously, Monserrat Bizarro also reported that Al can be doped into ZnO lattice with high concentrations [24]. This suggests that Al has a high solid solubility in ZnO.

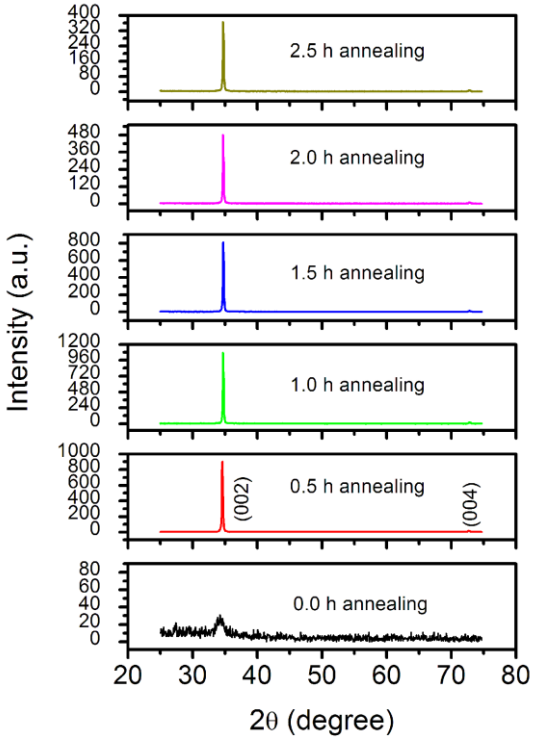

Fig. 1. XRD patterns of Al-Fe-Cl co-doped ZnO thin films with different annealing time (color online)

Fig. 2 displays the morphologies of ZnO films with different annealing times. When the sample is not annealed, there are many sheet-like structures on the film surface, similar to the ZnO-film morphologies reported by Kim et al. [20] and Rana et al. [25]. In this case, the spherical grains in the film are uniform but tiny. When the annealing time reaches 0.5 h, many pyramid-shaped grains appear on the film surface. Our previous study has shown that these pyramid-shaped grains are single-crystals and have high crystalline quality [21]. According to the size, grains can be divided into three types: small grains, medium grains and large grains. Apparently, proper annealing treatment is a necessary condition for the formation of pyramid-like nanostructures. Furthermore, it can be observed from the cross-sectional topography that the thickness of the sample subjected to the annealing treatment for 0.5 h decreased compared to the unannealed sample. This decrease in thickness may be attributed to two factors: (1) some components in the as-deposited film are removed in the form of H_2O, HCl, CO_2 or CO, NO_x, etc; (2) during the heat treatment, some Zn atoms at the bottom layer migrate to the surface and combine with oxygen to form pyramid-like nanostructures. In addition, it can be noticed that the grains in the polycrystalline layer at the bottom of the film slightly increase in size compared with those in the unannealed film. When the annealing time exceeds 1 h, the pyramid-like grains on the film surface exhibit obvious coalescence. The small and medium-sized grains gradually aggregate to and connect with the large grains, but the grain boundaries are still very clear.

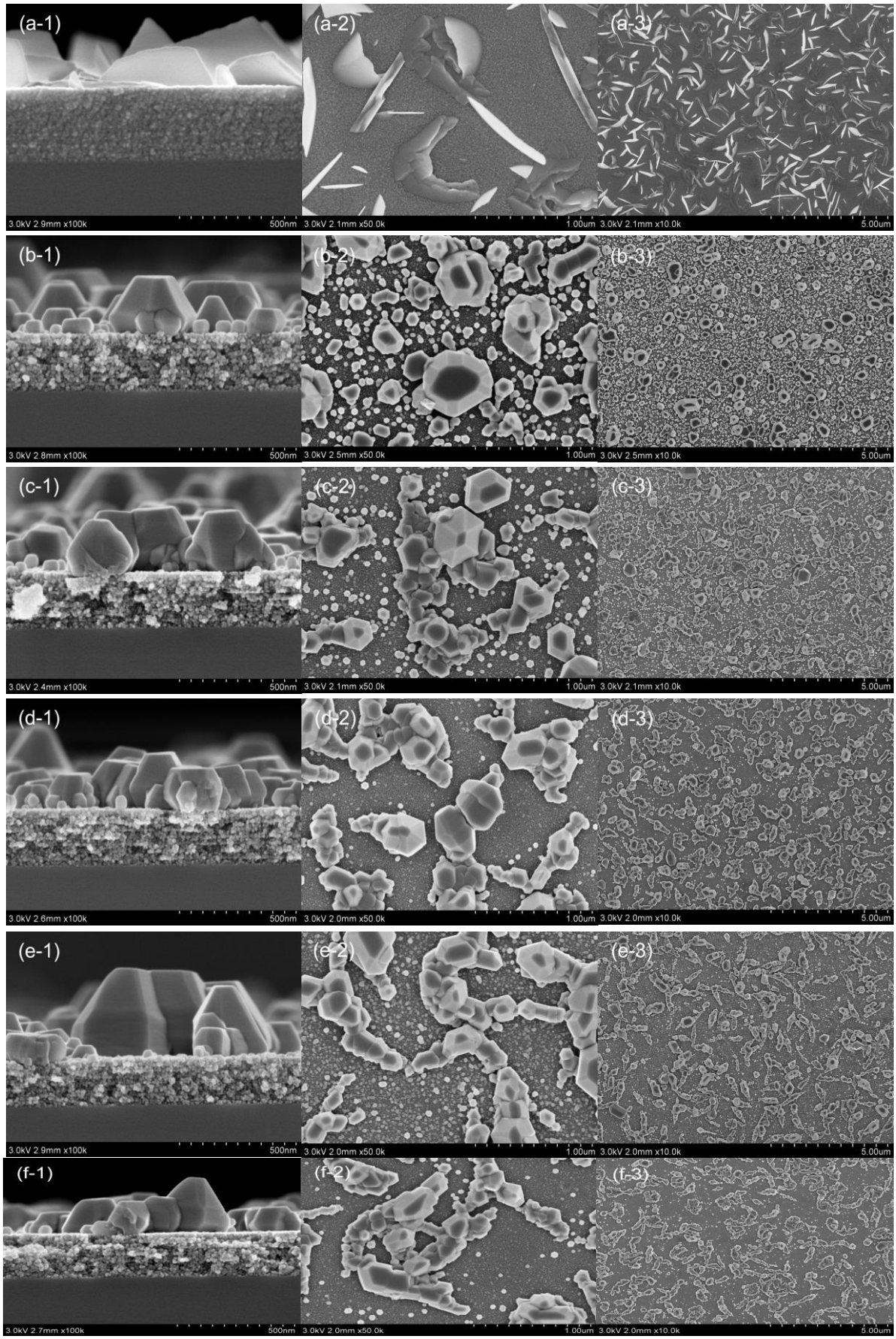

Fig. 2. SEM images of Al-Fe-Cl co-doped ZnO thin film with different annealing time: 0 h (a1-a3), 0.5 h (b1-b3), 1.0 h (c1-c3), 1.5 h (d1-d3), 2.0 h (e1-e3) and 2.5 h (f1-f3)

The aggregation behavior becomes more pronounced with further increase of annealing time. In this case, more of the polycrystalline ZnO layer at the film bottom is exposed due to small-sized and medium-sized grains migration. The above evolution is important because it will directly lead to the changes in the optical properties of the ZnO thin films described later. Previously, Tan et al. [26] observed that the coarsening behavior of ZnO films had a threshold temperature, which ranged from 600 to 700 °C; when the annealing temperature was lower than 800 °C, Ostwald ripening dominated the coarsening process of ZnO grains. For our samples, the annealing temperature was 450 °C, which is below the threshold temperature observed by Tan et al. However, the pyramid-like grains on the films surface also show obvious coalescence behavior. The difference in temperature threshold should originate from the different deposition methods of ZnO thin films [27]. Interestingly, at 450 °C, it is the pyramid-like grains in the upper layer, which show coalescence behavior, while the bottom ZnO polycrystalline layer does not show observable coarsening behavior. The reason why the coarsening behavior does not occur in the lower layer of the film is due to the Zener pining-effect [28]. EDS analysis has shown that the doped elements are mostly located in the bottom polycrystalline layer [21, 29], so the pinning effect occurs in the bottom polycrystalline layer rather than in the surface layer. Moreover, it is observed from Fig. 2 that the prolongation of annealing time hardly enhances the maximum height of the pyramid-like grain (about 350 nm), which may be caused by the limited diffusion length of Zn atoms. Moreover, the thickness of the bottom polycrystalline layer is always uniform and dense.

In order to determine the composition of the films, a representative sample was selected for EDS analysis. Fig. 3 illustrates the related EDS spectra. The elements of Zn, Si, Fe, Pt, Al, C, O and Cl are definitely found in the polycrystalline-layer at film bottom. The Si signal is from the substrate; the Pt signal is from the Pt particles intentionally sprayed before the detecting; the C signal should be from the CO_2 adsorbed on the sample surface, and the other signals are from the sample itself. Although the Cl signal is weak, it still exists. This indicates that during heat-treatment, Cl is not completely removed in the form of Cl_2 or/and HCl, but part of it enters into ZnO lattices as a replacer for oxygen atoms (Cl_O). However, for the pyramid-like ZnO grains, the detected signals of the doped elements are very low. This means that the doped elements of Al, Fe and Cl are all mainly located in the bottom polycrystalline layer [21]. This result is in agreement with that reported by Huang et al. [29]. Because the pyramid-like ZnO grains do not contain doped elements, they will not produce lattice distortion caused by doping, which make them have high crystal quality. The excellent crystal quality is the origin of the very high UV emission efficiency. In order to further understand the elemental distribution, the researchers collected mapping images on the selected rectangular area in Fig. 3(b). It can be confirmed from Fig. 4 that the doped elements of Al, Fe, and Cl are equably incorporated into the polycrystalline ZnO layer, and no aggregation state is observed.

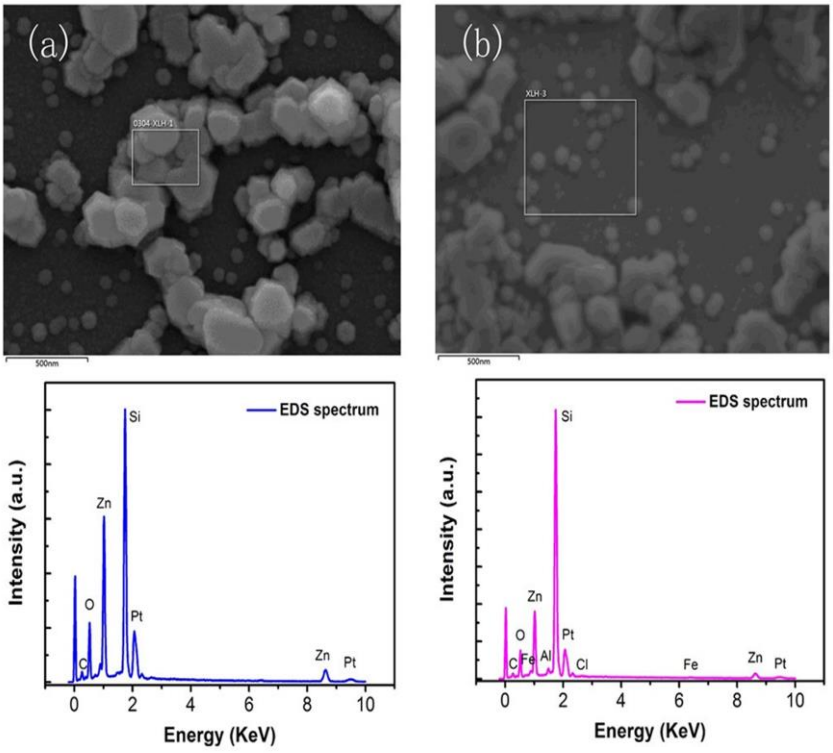

Fig. 3. EDS spectra for a typical sample (the scale bar is 500 nm) (color online)

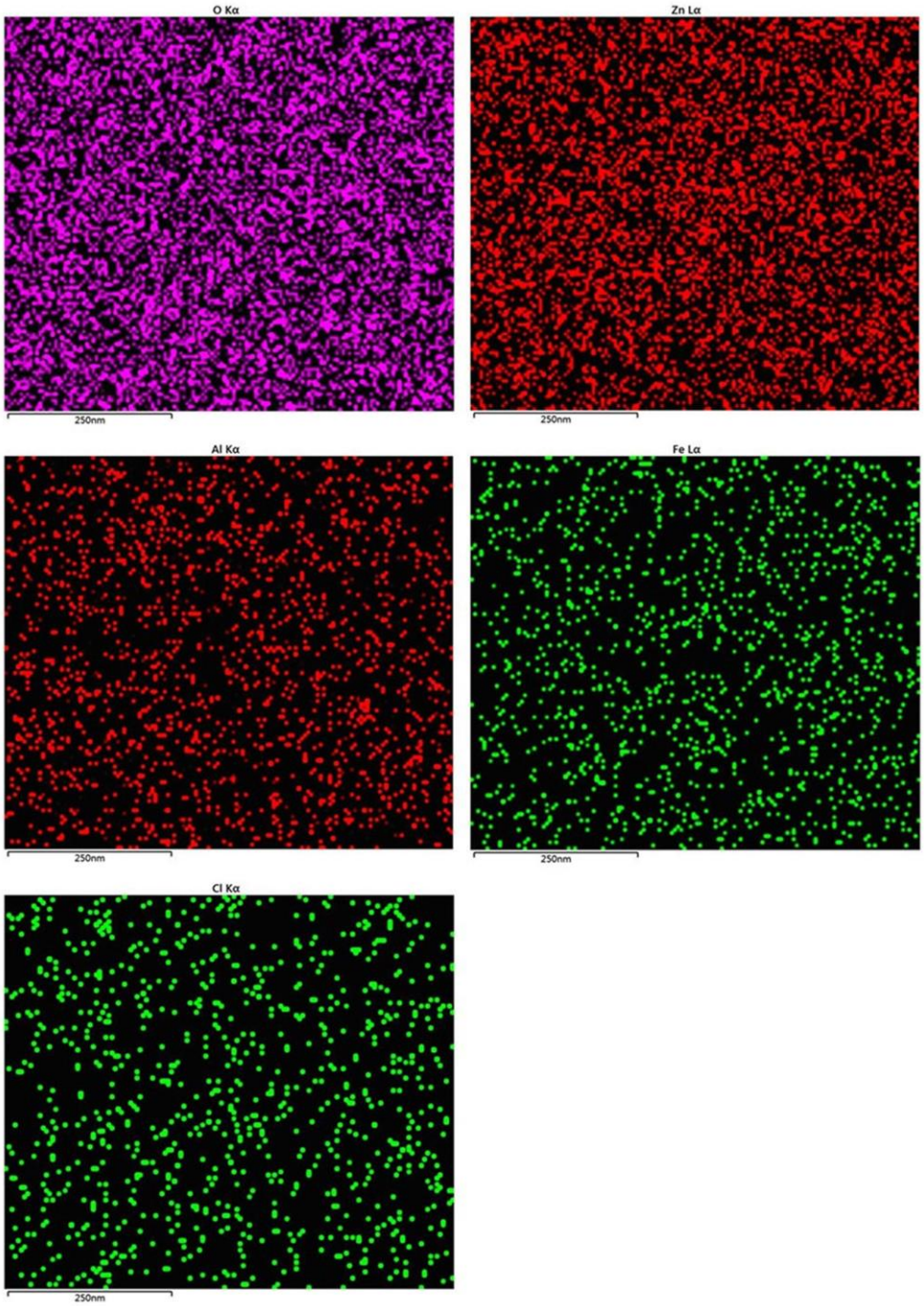

Fig. 4. Elemental mapping images of O, Zn, Al, Fe and Cl in the Al-Fe-Cl co-doped ZnO thin film (the scale bar is 250 nm) (color online)

To more understand the chemical state of the doped elements in the ZnO films, we measured the XPS spectra on a representative sample, which are displayed in Fig. 5. Fig. 5(a) shows that two geometrically symmetrical Zn 2p signal peaks are positioned at 1021.1 and 1044.2 eV, respectively, with a distance of 23.1 eV, implying that Zn^{2+} is the ionic state of Zn in the film. Fig. 5(b) presents the high-resolution O 1s peak that is not geometrically symmetric, implying that O on the ZnO surface is in different chemical states. By Gaussian fitting this signal peak, it can be seen that the signal peak of O 1s is composed of two subpeaks positioned at 530.3 and 532.0 eV respectively. The signal at 530.3 eV is derived from lattice oxygen, while the signal at 532.0 eV may have originated from oxygen-containing species adsorbed on the ZnO surface [29, 30]. Fig. 5(c) displays the signal peak of Al 2p at 74.0 eV, which is consistent with the binding energy of Al in Al_2O_3, indicating that Al exists in the +3 valence state [29]. It can be noticed from Fig. 5(d) that the 2p 3/2 and 2p 1/2 signal peaks of Fe are positioned at 710.6 and 724.7 eV, respectively, suggesting that Fe exists in the +3 valence state [30]. The signal peak of Cl 2p is located at 198.5 eV, which means that it exists in the -1 valence state.

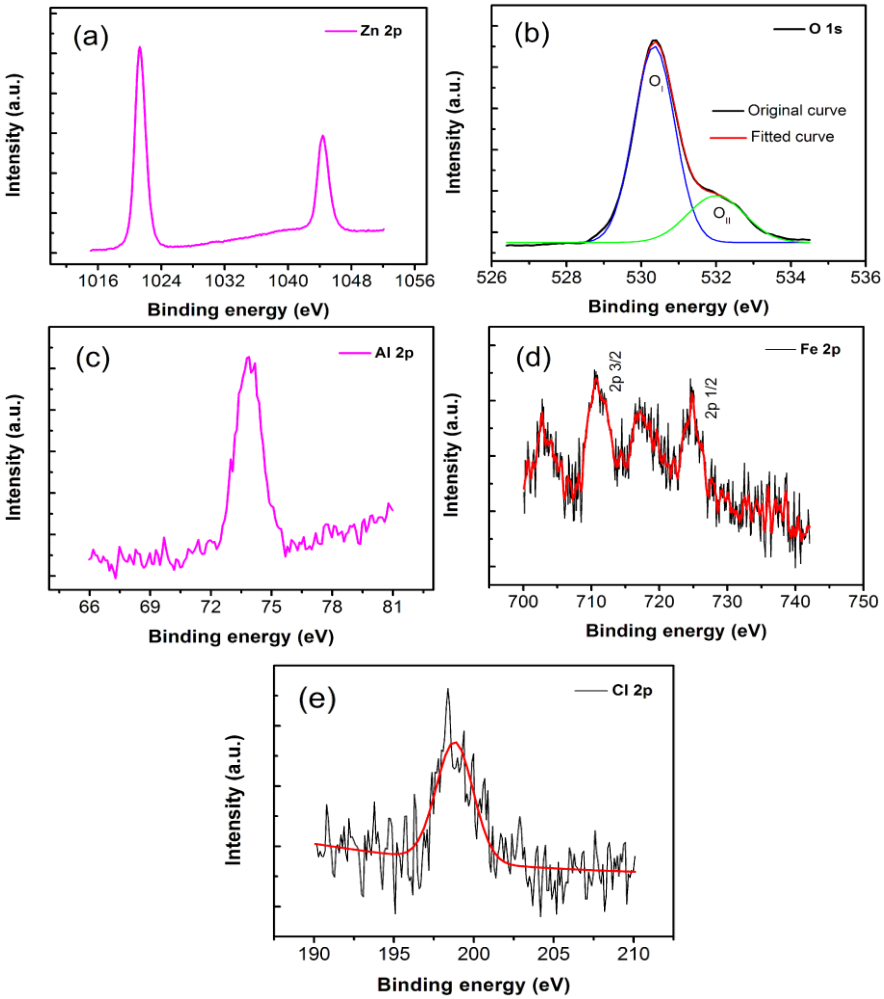

Fig. 5. Typical XPS spectra of Al-Fe-Cl co-doped ZnO thin film: (a) high-resolution spectrum of Zn 2p, (b) high-resolution spectrum of O 1s, (c) high-resolution spectrum of Al 2p, (d) high-resolution spectrum of Fe 2p and (e) high-resolution spectrum of Cl 2p (color online)

Fig. 6 presents the luminescence spectra of the films subjected to different annealing times. The unannealed sample shows a weak UV emission peak and relatively strong visible emission bands. It can be seen from the inset in Fig. 6 that the visible emissions contain not only green emission (about 510 nm), but also blue emission (about 450 nm) and red emission (690 nm). The blue-violet emission in ZnO is thought to be associated with zinc interstitials [31], while the green and red emissions may be derived from oxygen defects [32]. The XRD and PL results indicate that the unannealed Al-Fe-Cl co-doped ZnO film has poor crystalline quality and high point-defect density. The UV emission intensity rapidly increases with the prolongation of annealing time at first. Compared with the UV emission of pure ZnO film, that of the samples with pyramid-like grains on film surface is greatly enhanced. The enhanced UV emission originates from the highly crystalline pyramid-like nanostructures [21]. When the annealing time is 1 h, the UV emission intensity of the ZnO film reaches the maximum value. When the annealing time is more than 1 h, the UV emission intensity decreases. This decrease in UV emission intensity should be attributed to the evolution of film morphology derived by the increase of annealing time. It can be noticed from Fig. 2 that as the annealing time exceeds 1 h, the polycrystalline ZnO layer at the film bottom is more exposed due to the aggregation of pyramid-like grains on the surface. Therefore, part of the PL signal obtained in this case originates from the bottom polycrystalline ZnO layer. The crystal quality and UV emission efficiency of the polycrystalline ZnO layer are much lower than that of the pyramid-shaped single crystal ZnO grains in the upper layer. Therefore, the UV emission intensity decreases when the annealing time is too long. This means that choosing an appropriate annealing time is beneficial to obtain better optical quality for ZnO films with highly crystalline pyramid-like or columnar grains on the surface.

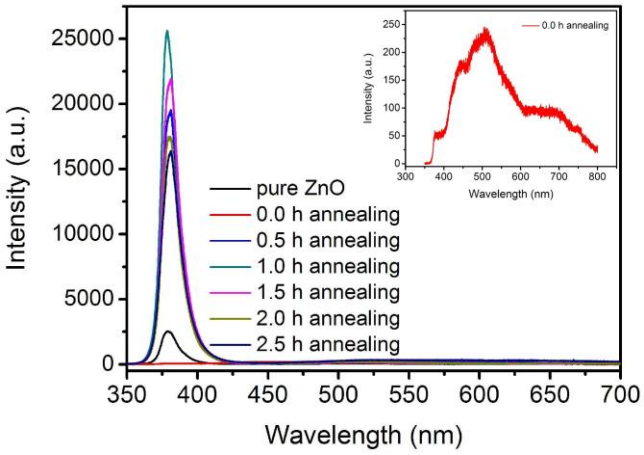

Fig. 6. Photoluminescence spectra of Al-Fe-Cl co-doped ZnO thin films with different annealing time (color online)

4. Conclusions

In this study, Al-Fe-Cl incorporated ZnO films were fabricated by spin-coating approach, and the influence of annealing-time on the surface morphology and luminescence behavior of the samples was explored. The results show that the annealed films have lots of pyramid-shaped grains on the surface; the cross-sectional morphology clearly reveals that the films are composed of the upper and lower layers. The annealing time shows different effects on the upper and lower layers of the ZnO films. Oswald ripening appeared in the upper pyramid-like structure, while the polycrystalline layer at the film bottom changed little due to the pinning effect of doping, and the coarsening behavior did not occur. The evolution of the surface morphology of the ZnO thin films has an important effect on the luminescence behavior. With the increase of annealing time, the UV emission is first greatly enhanced, which is derived from the occurrence of pyramid-like grains with highly crystalline quality; then, the UV emission decreases, which is ascribed to the coalescence of pyramid-like grains that exposes more of the bottom polycrystalline layer. The results are beneficial to develop high-quality ZnO materials for UV-emitting devices.

References

[1] M. A. M. Sarjidan, S. H. Basri, S. N. A. M. Johari, Q. A. Aziz, H. A. Rafaie, W. H. A. Majid, J. Optoelectron. Adv. M. **23**(11-12), 560 (2021).
[2] P. Narin, E. Kutlu-Narin, S. Kayral, R. Tulek, S. Gokden, A. Teke, S. B. Lisesivdin, Journal of Luminescence **251**, 119158 (2022).
[3] S. S. Mousavi, B. Sajad, Materials Research Bulletin **155**, 111950 (2022).
[4] Y. Li, Y. Huang, X. Wang, W. Liu, K. Yu, C. Liang, Journal of Physics and Chemistry of Solids **145**, 109540 (2020).
[5] H.-Y. Chen, B.-Y. Huang, H.-S. Koo, M.-T. Huang, Optik **220**, 164899 (2020).
[6] Y. Li, J. Feng, Y. Zhao, J. Wang, C. Xu, Applied Surface Science **599**, 153969 (2022).
[7] H. Ferhati, F. Djeffal, Superlattices and Microstructures **134**, 106225 (2019).
[8] Z. G. Bafghi, N. Manavizadeh, Optics and Laser Technology **129**, 106310 (2020).
[9] V. Mirkhani, K. Yapabandara, S. Wang, M. P. Khanal, S. Uprety, M. S. Sultan, B. Ozden, A. C. Ahyi, M. C. Hamilton, M. H. Sk, M. Park, Thin Solid Films **672**, 152 (2019).
[10] T. K. O. Vu, M. T. Tran, E. K. Kim, Journal of Alloys and Compounds **924**, 166531 (2022).
[11] J. Fang, J.-J. Xue, R.-P. Xiao, X. Chen, Y.-M. Guo, J.-M. Song, Journal of Environmental Chemical Engineering **10**, 108334 (2022).
[12] S. Nachimuthu, S. Thangavel, K. Kannan, V. Selvakumar, K. Muthusamy, M. R. Siddiqui, S. M. Wabaidur, C. Parvathiraja, Chemical Physics Letters **804**, 139907 (2022).
[13] S. Abdolalian, M. Taghavijeloudar, Journal of Cleaner Production **365**, 132833 (2022).
[14] P. F. Ji, Y. Li, F. Q. Zhou, Y. L. Song, H. C. Huang, Materials Letters **262**, 127028 (2020).
[15] S. H. Moon, J. Jeong, G. W. Kim, D. K. Jin, Y.-J. Kim, J. K. Kim, K. S. Kim, G. Kim, Y. J. Hong, Current Applied Physics **20**, 352 (2020).
[16] J. H. Lim, J. H. Shim, J. H. Choi, J. Joo, K. Park, H. Jeon, M. R. Moon, D. Jung, H. Kim, H.-J. Lee, Applied Physics Letters **95**, 012108 (2009).
[17] D.-T. Phan, G.-S. Chung, Applied Surface Science **257**, 3285 (2011).
[18] J. Sengupta, R. K. Sahoo, C. D. Mukherjee, Materials Letters **83**, 84 (2012).
[19] R. Yatskiv, J. Grym, Š. Kučerová, S. Tiagulskyi, O. Černohorský, N. Bašinová, J. Veselý, Journal of Sol-Gel Science and Technology **102**, 447 (2022).
[20] D. Kim, E. Jo, J.-Y. Leem, Phys. Status Solidi A **218**, 2000698 (2021).
[21] L. Xu, X. Wang, G. Zheng, J. Su, Surfaces and Interfaces **27**, 101535 (2021).
[22] Y. Vijayakumar, P. Nagaraju, V. Yaragani, S. R. Parne, N. S. Awwad, M. V. R. Reddy, Physica B **581**, 411976 (2020).
[23] A. Goktas, F. Aslan, B. Yeşilata, İ. Boz, Materials Science in Semiconductor Processing **75**, 221 (2018).
[24] M. Bizarro, Applied Catalysis B: Environmental **97**, 198 (2010).
[25] V. S. Rana, J. K. Rajput, T. K. Pathak, L. P. Purohit, Journal of Alloys and Compounds **764**, 724 (2018).
[26] S. T. Tan, X. W. Sun, X. H. Zhang, S. J. Chua, B. J. Chen, C. C. Teo, Journal of Applied Physics **100**, 033502 (2006).
[27] M. W. Zhu, J. Gong, C. Sun, J. H. Xia, X. Jiang, Journal of Applied Physics **104**, 073113 (2008).
[28] K. Thongsuriwong, P. Amornpitoksuk, S. Suwanboon, J. Sol-Gel Sci. Technol. **62**, 304 (2012).

[29] N. Huang, C. Sun, M. Zhu, B. Zhang, J. Gong, X. Jiang, Nanotechnology **22**, 265612 (2011).
[30] S. Baek, J. Song, S. Lim, Physica B **399**, 101 (2007).
[31] B. Jin, D. Wang, Journal of Luminescence **132**, 1879 (2012).
[32] Y. Yang, S. Li, F. Liu, N. Zhang, K. Liu, S. Wang, G. Fang, Journal of Luminescence **186**, 223 (2017).

*Corresponding author: congyu3256@sina.com